Journal of Photonics for Energy

PhotonicsforEnergy.SPIEDigitalLibrary.org

Organic solar cells based on acceptor-functionalized diketopyrrolopyrrole derivatives

Sanjay S. Ghosh
Luis A. Serrano
Bernd Ebenhoch
Vincent M. Rotello
Graeme Cooke
Ifor D. W. Samuel

SPIE.

Organic solar cells based on acceptor-functionalized diketopyrrolopyrrole derivatives

Sanjay S. Ghosh,[a,†] Luis A. Serrano,[b,†] Bernd Ebenhoch,[a] Vincent M. Rotello,[c] Graeme Cooke,[b,*] and Ifor D. W. Samuel[a,*]

[a]University of St. Andrews, Organic Semiconductor Centre, SUPA, School of Physics and Astronomy, North Haugh, St. Andrews Fife, KY16 9SS, United Kingdom

[b]University of Glasgow, Glasgow Centre for Physical Organic Chemistry, School of Chemistry, Glasgow, G12 8QQ, United Kingdom

[c]University of Massachusetts Amherst, Department of Chemistry, 710 N. Pleasant Street, Amherst, Massachusetts 01003, United States

Abstract. The synthesis and characterization of three solution processable diketopyrrolopyrrole (DPP) derivatives featuring acceptor units attached to the core by alkyne linker units is reported. Cyclic voltammetry and density functional theory calculations indicate that the DPP derivatives possess similar HOMO and LUMO energies. Solar cells were fabricated by blending the synthesized DPP derivatives with [6,6]-phenyl-C71-butyrate methyl ester. The influence of donor: acceptor blend ratio, film thickness, annealing temperature, and annealing time on device performance was studied. Differences in device performance were related to atomic force microscopy measurements of the films. The highest power conversion efficiency of 1.76% was achieved for the DPP derivative functionalized with an aldehyde electron-withdrawing group with a 1:0.7 donor:acceptor ratio when the active layer was annealed for 10 min at 110°C.
 [DOI: 10.1117/1.JPE.5.057215]

Keywords: diketopyrrolopyrrole; acceptor-functionalized; small molecule; solar cell; [6,6]-phenyl-C71-butyrate methyl ester.

Paper 14082SS received Oct. 19, 2014; accepted for publication Apr. 16, 2015; published online Jun. 12, 2015.

1 Introduction

Solution-processed organic solar cells based upon bulk heterojunction (BHJ) architectures continue to attract significant interest due to their potential for low-cost fabrication by simple printing techniques and the ability to produce flexible and lightweight devices.[1] Significant progress was achieved in the development of BHJs featuring reasonable power conversion efficiencies (PCEs) from conjugated polymers as the donor component and methyl [6,6]-phenyl-C_{71}-butyrate methyl ester ($PC_{71}BM$) as the acceptor.[2] However, conjugated polymers have some important drawbacks, including limited batch-to-batch reproducibility and laborious purification, which limit their large-scale synthesis. BHJs featuring small molecule donors have emerged as important alternatives to conjugated polymer-based solar cells due to their better synthetic reproducibility, well-defined structure, and ability to be produced with high purity.[3–8] Significant progress has recently been made in the reported power conversion efficiencies of small molecule-based devices, which has resulted in systems of this type becoming viable alternatives for fabricating active layers within BHJs.

In this article, we describe the synthesis and characterization of three small molecule diketopyrrolopyrrole (DPP) derivatives (DPP-BZ, DPP-ES, and DPP-AM) and their subsequent fabrication as BHJ devices with $PC_{71}BM$. DPP was selected as the core moiety for this

*Address all correspondence to: Graeme Cooke, E-mail: Graeme.Cooke@glasgow.ac.uk and Ifor D. W. Samuel, E-mail: idws@standrews.ac.uk

†Authors contributed equally.

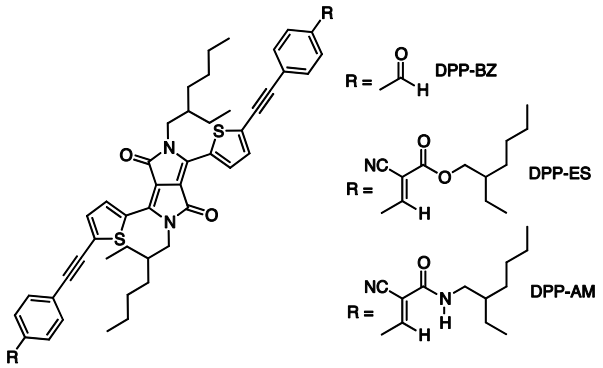

Fig. 1 Structures of DPP-BZ, DPP-ES, and DPP-AM.

study in view of its convenient synthesis, excellent light absorption properties, good photochemical/thermal stability, and excellent charge carrier mobility.[9–12] We have further functionalized the DPP core with electron-withdrawing aldehyde (DPP-BZ), cyanoacrylic ester (DPP-ES), and cyanoacrylic amide (DPP-AM) units (Fig. 1) in an effort to tune the optical and redox properties of the DPP core. Furthermore, for DPP-AM and DPP-ES, we have included 2-ethylhexyl side chains to promote good solubility of these derivatives and, in the case of DPP-AM, an amide unit that could have the propensity to participate in intermolecular hydrogen bonding.

2 Experimental Details

2.1 *Synthesis*

All melting points are uncorrected. The NMR spectra were recorded on a Bruker AVIII 500 MHz spectrometer as $CDCl_3$ solutions. The ^1H and ^{13}C spectra were recorded at 500 and 125 MHz, respectively, with either residual nondeuterated chloroform [δ 7.26 (^1H) and δ 77.0 (^{13}C)] or tetramethylsilane as the internal standard. Mass spectrometry measurements electrospray ionisation (ESI) were undertaken using a Bruker microTOFq high-resolution mass spectrometer. Reactions were performed under an atmosphere of nitrogen (oxygen-free) using oven-dried glassware (dried for 24 h at 100°C). Dry solvents were obtained using the Pure-Solv™ Solvent Purification System (Innovative Technology). 2-ethylhexyl-2-cyanoacetate,[13] *N*-(2-ethylhexyl)-2-cyanoacetamide,[14] and DPP-Br_2[15] were synthesized according to literature procedures.

2.1.1 *DPP-BZ*

DPP-Br_2 (300 mg, 0.44 mmol) and 4-ethynylbenzaldehyde (126 mg, 0.97 mmol) were dissolved in dry tetrahydrofuran (10 mL) and dry triethylamine (10 mL) under N_2, and the solution was degassed with N_2 for 15 min. $Pd(PPh_3)_2Cl_2$ (18 mg, 0.026 mmol) and CuI (2.5 mg, 0.013 mmol) were then added and the solution was stirred at room temperature overnight. The reaction was then diluted with diethyl ether (100 mL) and washed with brine (3×100 mL). The organic layer was dried with $MgSO_4$, filtered, and the solvent removed under reduced pressure. The crude product was purified by column chromatography [SiO_2, 100% dichloromethane (DCM)] to give the desired product as a blue solid (261 mg, 76%), with a melting point (m.p.) 211°C to 212°C. ^1H NMR (500 MHz, $CDCl_3$) δ: 0.77 to 0.87 (12H, m, CH_3, 1.15 to 1.35 (16H, m, CH_2, 1.82 (2H, m, CH), 3.93 (4H, m, CH_2, 7.35 (2H, d, $J = 4.1$ Hz, ArH), 7.61 (4H, d, $J = 8.2$ Hz ArH), 7.81 (4H, d, $J = 8.2$ Hz ArH), 8.83 (2H, d, $J = 4.1$, ArH), 9.95 (1H, s, CH=O); ^{13}C NMR (125 MHz, $CDCl_3$) δ: 10.4, 14.0, 23.0, 23.6, 28.3, 30.1, 39.1, 46.6, 86.0, 96.6, 109.16, 127.6, 128.4, 129.6, 131.4, 132.0, 133.8, 135.5, 135.9, 139.5, 161.4, 191.2; high resolution mass spectrometry m/z [ESI ($M + Na^+$)] 803.2913 ($C_{48}H_{48}N_2S_2O_4Na$ requires 803.2948).

2.1.2 *DPP-ES*

DPP-BZ (260 mg, 0.33 mmol), piperidine (7 μL, 0.066 mmol), acetic acid (30 μL, 0.53 mmol), and $MgSO_4$ (33 mg, 0.13 mmol) were dissolved in dry toluene (5 mL) under

N_2. 2-ethylhexyl-2-cyanoacetate (0.14 mg, 0.73 mmol) was added to the mixture and the solution was heated at 110°C for 4 h. After cooling to room temperature, the mixture was diluted with DCM (50 mL) and brine (50 mL), and the aqueous layer was washed with DCM (3×50 mL). The organic extracts were combined, dried with $MgSO_4$, filtered, and the solvent was removed under reduced pressure. The crude product was purified by column chromatography (SiO_2, 100% DCM) to give the desired product as a blue solid (258 mg, 69%), m.p. 219°C to 220°C. ^{1}H NMR (500 MHz, $CDCl_3$) δ: 0.78 to 0.91 (24H, m, CH_3, 1.14 to 1.43 (32H, m, CH_2, 1.65 (2H, m, CH), 1.83 (2H, m, CH), 3.95 (4H, m, CH_2, 4.18 (4H, m, CH_2, 7.37 (2H, d, $J = 4.1$ Hz, ArH), 7.57 (4H, d, $J = 8.4$ Hz, ArH), 7.93 (4H, d, $J = 8.4$ Hz, ArH), 8.14 (1H, s, CH=C) 8.84 (2H, d, $J = 4.1$, ArH); ^{13}C NMR (125 MHz, $CDCl_3$) δ: 10.5, 11.0, 14.0, 22.9, 23.0, 23.6, 23.8, 28.3, 28.9, 30.2, 30.3, 38.8, 39.2, 46.2, 69.2, 86.4, 96.8, 103.7, 109.2, 115.2, 127.2, 127.6, 131.0, 131.5, 131.6, 132.1, 133.9, 135.6, 139.6, 153.3, 161.5, 162.4. MS (MALDI) m/z 1138.6 (M^+).

2.1.3 *DPP-AM*

DPP-BZ (260 mg, 0.33 mmol), piperidine (7 μL, 0.066 mmol), acetic acid (30 μL, 0.53 mmol), and $MgSO_4$ (33 mg, 0.13 mmol) were dissolved in dry toluene (40 mL) under N_2. *N*-(2-ethylhexyl)-2-cyanoacetamide (0.14 mg, 0.73 mmol) was added to the mixture, and the solution was heated at 110°C for 4 h. After cooling to room temperature, the mixture was diluted with DCM (50 mL) and brine (50 mL), and the aqueous layer was washed with DCM (3×50 mL). The organic extracts were combined, dried with $MgSO_4$, filtered, and the solvent removed under reduced pressure. The crude product was purified by column chromatography (SiO_2, 100% DCM) to give the desired product as a blue solid (100 mg, 26%). m.p. 219°C to 220°C. ^{1}H NMR (500 MHz, $CDCl_3$) δ: 0.88 to 0.98 (24H, m, CH_3), 1.24 to 1.45 (32H, m, CH_2), 1.59 (2H, m, CH), 1.92 (2H, m, CH), 3.41 (4H, m, CH_2), 4.05 (4H, m, CH_2), 6.36 (1H, t, $J = 5.8$ Hz, NH), 7.47 (2H, d, $J = 4.1$ Hz, ArH), 7.66 (4H, d, $J = 8.4$ Hz, ArH), 7.97 (4H, d, $J = 8.4$ Hz, ArH), 8.33 (1H, s, CH=C), 8.94 (2H, d, $J = 4.1$, ArH); ^{13}C NMR (125 MHz, $CDCl_3$) δ: 10.5, 10.9, 14.0, 22.9, 23.0, 23.6, 23.8, 28.3, 28.9, 30.2, 30.4, 39.2, 39.4, 46.2, 68.2, 77.6, 86.0, 96.9, 104.8, 109.2, 117.0, 126.6, 127.7, 130.6, 131.4, 132.0, 132.1, 133.8, 135.6, 139.5, 151.3, 159.9, 161.5. MS (MALDI) m/z 1136.6 (M^+).

2.2 *Characterization*

2.2.1 *Electrochemistry*

Cyclic voltammetry (CV) experiments were performed using a CH Instruments 440A electrochemical workstation. All measurements were undertaken under an oxygen-free nitrogen atmosphere. A solution of electrochemical grade tetrabutylammonium hexafluorophosphate dissolved in dry DCM (0.1 M) was employed as the supporting electrolyte. A platinum disc working electrode, a platinum wire counter electrode, and a silver wire pseudo-reference electrode were used for all measurements. The half-wave potentials were referenced to ferrocene (Fc) (internal reference) with the Fc/Fc+ redox couple adjusted to 0 V. The HOMO and LUMO energies were estimated from the CV derived half-wave potentials of the first oxidation and reduction waves, respectively, using the following equations:

$$E_{(\mathrm{HOMO})} = (-4.8) - [E_{1/2(\mathrm{ox})}],$$

$$E_{(\mathrm{LUMO})} = (-4.8) - [E_{1/2(\mathrm{red})}],$$

where -4.8 eV is the $E_{(\mathrm{HOMO})}$ for Fc against the vacuum.[16]

2.2.2 *Density functional theory calculations*

Calculations were performed using the Spartan '08 software suite.[17] Molecular geometries were initially optimized semi-empirically (AM1) and then reoptimized using density functional theory (DFT) (B3LYP/6-31G*). The optimized structures were shown to be local minima as the

vibrational frequencies in the optimized geometries did not generate imaginary frequencies. To facilitate the convergence of the geometry optimizations, the 2-ethylhexyl side chains of the DPP derivatives were replaced by methyl units.

2.2.3 *Solar cell fabrication and characterization*

Solar cells were fabricated on patterned indium tin oxide coated glass substrates purchased from Xinyan Technology Ltd. (10 to 13 ohm/sq). The substrates were cleaned by ultra-sonication in acetone and isopropyl alcohol successively for 10 min each. The dried substrates were then treated with oxygen plasma for 3 min. The hole conducting poly(3,4-ethylenedioxythiophene)-poly(styrenesulfonate) layer (CLEVIOS™ P VP AI 4083) was then spin-coated at 4000 rpm to obtain films of 30 nm thickness and was annealed on a hot plate at 140°C for 10 min to remove the residual water. The dried substrates were then transferred into a nitrogen glove box to deposit the active layer made from a blend of the DPP material with $PC_{71}BM$ (99% purity from Solenne) spin-coated at 1000 rpm from the chloroform solution. These were then annealed at 110°C for 10 min. The solution concentration was varied to provide films of different thicknesses. Thereafter, a 15 nm calcium layer followed by a 100 nm aluminum layer were evaporated at a pressure of 2×10^{-6} mbar. Active areas of devices (2×4 mm^2) were defined by a shadow mask. The devices were then encapsulated by using UV-curable epoxy to glue a glass slide to the top of the device.

The current–voltage (J–V) characteristics were measured in ambient conditions under illumination at 100 mW/cm^2 intensity by using a Keithley 2400 source measure unit and a Science-Tech, SS150 solar simulator. The light intensity at the test surface was measured using a Newport Oriel reference cell. For J–V measurement of the solar cells, a shadow mask equal to the size of the test pixel was used to avoid the generation of charge carriers by photons absorbed outside the cell area. Absorption spectra were recorded by using a Cary 300 spectrophotometer. Atomic force microscopy (AFM) images were recorded by using a Veeco diCaliber instrument in the tapping mode. All the film thicknesses were measured using a Dektak 150 surface profiler. External quantum efficiency (EQE) measurement was performed with an incident photon to charge carrier efficiency setup, which consists of a xenon lamp, a photodiode calibrated by the National Physical Laboratory (UK), Keithley 6517A picoammeter, and a TMc300 monochromator.

3 Results and Discussion

The synthesis of DPP-BZ, DPP-ES, and DPP-AM from DPP-Br_2 is outlined in Fig. 2. To help promote planarity of the derivatives, the electron-withdrawing moieties[18–22] were introduced using Sonogashira-coupling reactions of DPP-Br_2 and 4-ethynylbenzaldehyde.[23] Further, Knoevenagel condensation of DPP-BZ with 2-ethylhexyl-2-cyanoacetate and *N*-(2-ethylhexyl)-2-cyanoacetamide afforded DPP-ES and DPP-AM, respectively. CV was used to estimate the HOMO and LUMO energies of the DPP derivatives from the half-wave potentials of their redox waves (Table 1). The CV of DPP-BZ is provided in Fig. 3. The electrochemical data reveal similar oxidation and reduction potentials for all three materials, indicating that the differing groups at the termini of the molecules play a minimal role in modulating the ionization potential and electron affinity of these derivatives.

DFT calculations performed on the DPP derivatives indicated a planar structure for all three derivatives, and the HOMO/LUMO energy levels are shown in Table 1. The HOMO/LUMO distributions are shown in the contour maps provided in Fig. 4. For all derivatives, the HOMO is mainly localized on the DPP core and the directly attached alkyne residue. The LUMO maps are also similar for each derivative, and partially extend onto the electron-withdrawing aldehyde moieties of DPP-BZ and the cyano residues of DPP-ES and DPP-AM. The calculated LUMO/HOMO energy values are in good agreement with the CV-estimated values, further indicating that the differing electron-withdrawing units had surprisingly little effect in perturbing the electronic properties of these systems (Table 1). The optical band gaps (E_{opt}) obtained from solution UV-Vis spectra of the DPP derivatives are close to the HOMO-LUMO gaps provided by DFT and electrochemistry (~1.8 eV).

The absorption spectra of the materials in thin films are shown in Fig. 5. They show an onset around 750 nm and peaks in the range of 600 to 700 nm. The absorption peaks of the films are

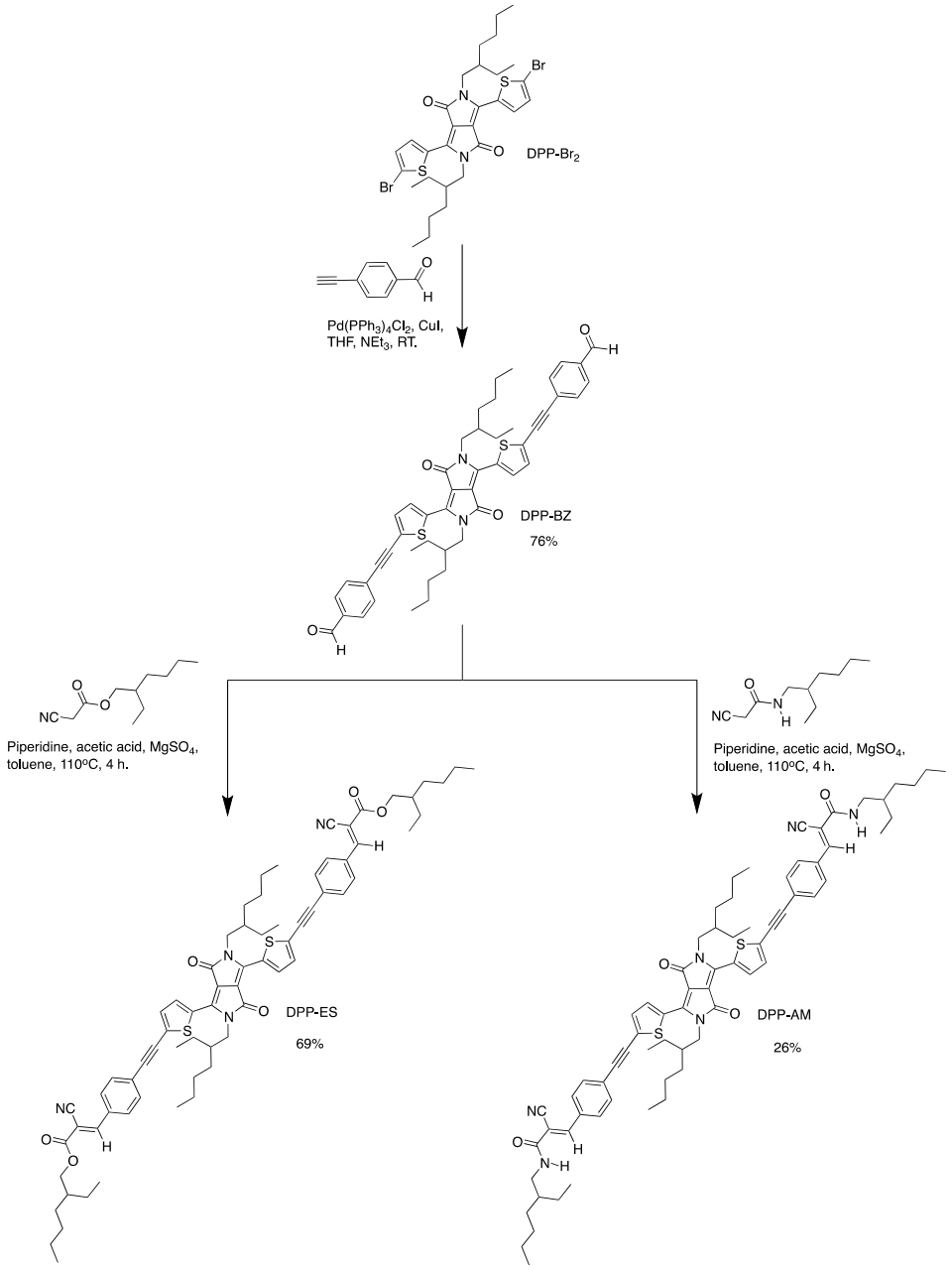

Fig. 2 Synthesis of the compounds used in this study.

Table 1 Estimated HOMO and LUMO energies derived from half-wave potentials from cyclic voltammetry measurements. The concentration of the diketopyrrolopyrrole (DPP) derivative was 5×10^{-4} M in DCM. HOMO and LUMO values in brackets are derived from DFT calculations.

	$E_{1/2(ox)}$ (V)	$E_{1/2(red)}$ (V)	HOMO (eV)	LUMO (eV)
DPP-BZ	0.54	−1.42	−5.3 (−5.2)	−3.4 (−3.2)
DPP-ES	0.53	−1.46	−5.3 (−5.2)	−3.3 (−3.3)
DPP-AM	0.53	−1.42	−5.3 (−5.1)	−3.4 (−3.2)

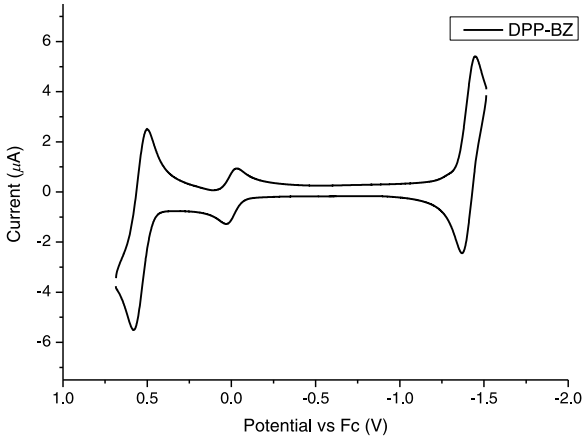

Fig. 3 Cyclic voltammetry of DPP-BZ, measured at a concentration of 5×10^{-4} M in dichloromethane.

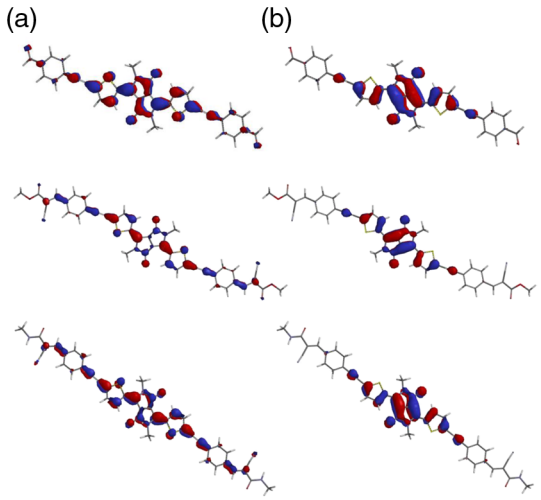

Fig. 4 DFT-predicted (a) LUMO and (b) HOMO maps for DPP-BZ (top), DPP-ES (middle), and DPP-AM (bottom).

redshifted by ~40 nm compared to that in solution (data not shown). This is consistent with a more rigid and ordered structure in the solid state.[24,25] In addition to this, significant broadening of the absorption in the region of 300 to 450 nm was also observed. The absorption of DPP-ES and DPP-AM is slightly redshifted compared to DPP-BZ largely due to the presence of the CN group in DPP-ES and DPP-AM.

Solar cells containing each of the DPP materials as the electron donor blended with $PC_{71}BM$ as the electron acceptor were fabricated to evaluate the photovoltaic properties of the materials. The J–V characteristics of the devices using DPP-ES:$PC_{71}BM$ and DPP-AM:$PC_{71}BM$ blends as the photoactive layer [1 : 0.7 donor:acceptor (D:A) ratio and 83 nm thick] are shown in Fig. 6. Both the devices show poor performance with low short circuit current density (J_{sc}) and, hence, very low overall PCE of 0.08 to 0.10%.

The poor device performance was investigated by recording AFM images. Figure 7 shows that both active layers have similar morphologies with domains around 150 to 250 nm in diameter. Smaller aggregates are desirable allowing increased interfacial area and better charge separation.[26] This, in general, results in an increase in J_{sc} and hence an enhanced overall device performance.[27] The domain sizes in the present study are much larger than the optimal required for efficient exciton dissociation. This limits the overall performance of these devices. In addition, there was substantial surface roughness of the blend films: the RMS roughness values were

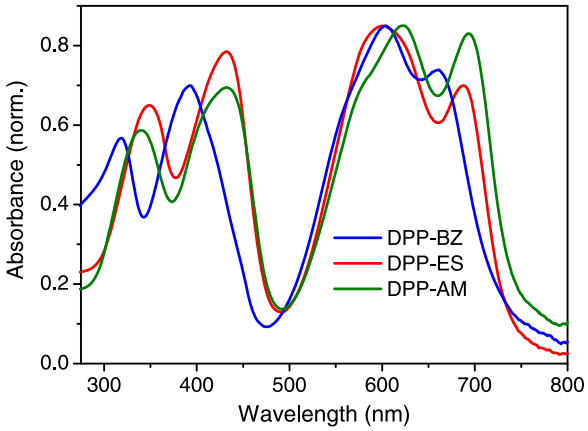

Fig. 5 Absorption spectra of films of DPP derivatives.

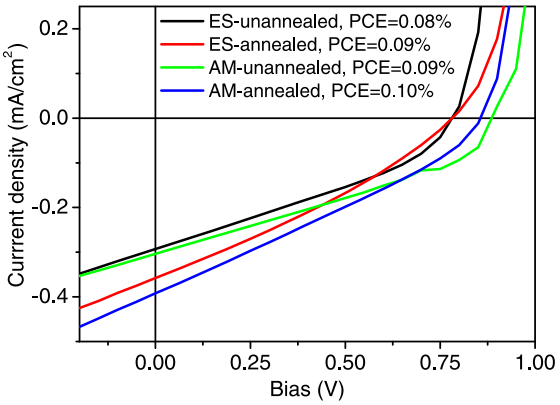

Fig. 6 *J*–V characteristics of the devices by using DPP-ES:[6,6]-phenyl-C71-butyrate methyl ester ($PC_{71}BM$) and DPP-AM:$PC_{71}BM$ blends as the photoactive layer.

18.6 nm for DPP-ES:$PC_{71}BM$ and 19.6 nm for DPP-AM:$PC_{71}BM$ in as coated films. Upon annealing, the roughness does not significantly change. This roughness is undesirably high as it is known that smooth active layers are essential for optimum device performance.[28] A possible reason for the larger than desirable phase separation could be the intramolecular dipoles due to the cyano units. Dipole–dipole interactions could facilitate aggregation and discourage mixing with the acceptor.[29]

Figure 8 shows the *J*–*V* characteristics of the devices using a DPP-BZ:$PC_{71}BM$ blend as the photoactive layer under 1 sun illumination. The effect of D:A blend ratios on device performance was investigated for films of thickness 83 nm and the results are shown in Table 2. As the acceptor proportion decreases, the highest PCE was obtained for a 1:0.7 D:A ratio annealed at 110°C for 10 min. With a 1:2 D:A ratio, an overall PCE of 0.73% was obtained with a short-circuit current density of 2.45 mA/cm^2, an open circuit voltage (V_{oc}) of 0.79 V, and a fill factor (FF) of 37.4%. Further reductions in $PC_{71}BM$ content reduces the performance. With a 1:0.6 blend, a PCE of 1.44% was obtained.

AFM measurements were performed to investigate the effect of the D:A ratio on the blend film morphology (Fig. 9). Blend films with a 1:2 D:A ratio show aggregates of size 150 to 250 nm in diameter. Upon reducing the content of $PC_{71}BM$ in the blend films, the domain size decreases considerably. It is, therefore, clear that with reduced $PC_{71}BM$ content, the donor and acceptor are more homogeneously mixed. This is crucial for efficient charge separation in BHJ devices.[30] Upon thermal annealing, the pore size and pore density at the film surface decreased. Thermal annealing also helps in the removal of air voids formed due to inherent instability involved in the spin-coating process. For a 1:0.7 D:A ratio, the homogeneity of

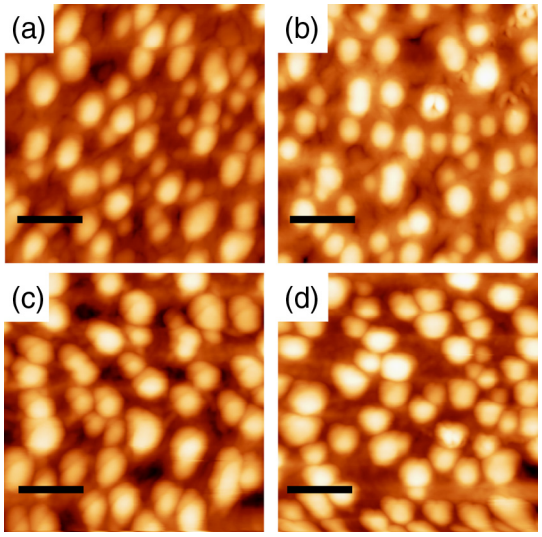

Fig. 7 Atomic force microscopy (AFM) images. The z-scale is 95 nm for (a) as coated and (b) annealed DPP-ES:$PC_{71}BM$ blends. The z-scale is 110 nm for (c) as coated and (d) annealed DPP-AM:$PC_{71}BM$ blends. The scale bar shows a length of 0.5 μm.

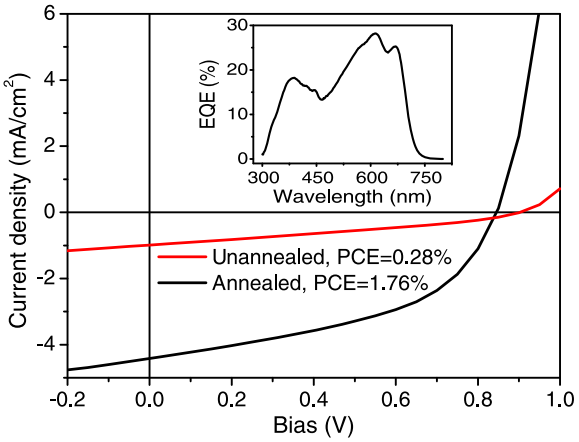

Fig. 8 *J*–V characteristics of the devices using DPP-BZ:$PC_{71}BM$ blend as the photoactive layer. Inset shows the external quantum efficiency of best performing device having PCE = 1.76%.

Table 2 Performance parameters of the devices, using DPP-BZ:$PC_{71}BM$ blends as the photoactive layer of different donor:acceptor (D:A) ratios.

D:A ratio	PCE (%)	J_{sc} (mA/cm^2)	V_{oc} (V)	FF (%)
1:2	0.73	2.45	0.79	37.4
1:1.5	0.83	2.79	0.79	37.7
1:1	1.05	3.23	0.77	41.9
1:0.7	1.76	4.42	0.85	47.2
1:0.6	1.44	3.90	0.81	45.5

the film is considerably enhanced and the RMS roughness reduces considerably upon thermal annealing. For the as coated film, the RMS roughness is 7.4 nm compared to 4.9 nm after thermal annealing. A significant change in the height profile upon thermal annealing [Fig. 9(g)] shows enhanced homogeneity and improved surface smoothness of the blend films due to thermal annealing. The reverse saturation current is a measure of the number of carriers that can overcome the energetic barrier created by the p-n junction in the reverse bias condition.[31] In the device with a 1:0.7 D:A, the rectification ratio improved by a factor of 29 compared to that of a 1:2 D:A ratio device at ± 1 V. This is an indication of the large reduction in reverse saturation current in the devices with lower $PC_{71}BM$ content. For further reduced ratios of $PC_{71}BM$, the films were smoother, but the solar cell performance decreased. The effect of annealing conditions was also explored. Devices annealed for 5 and 15 min at 110°C (1:0.7

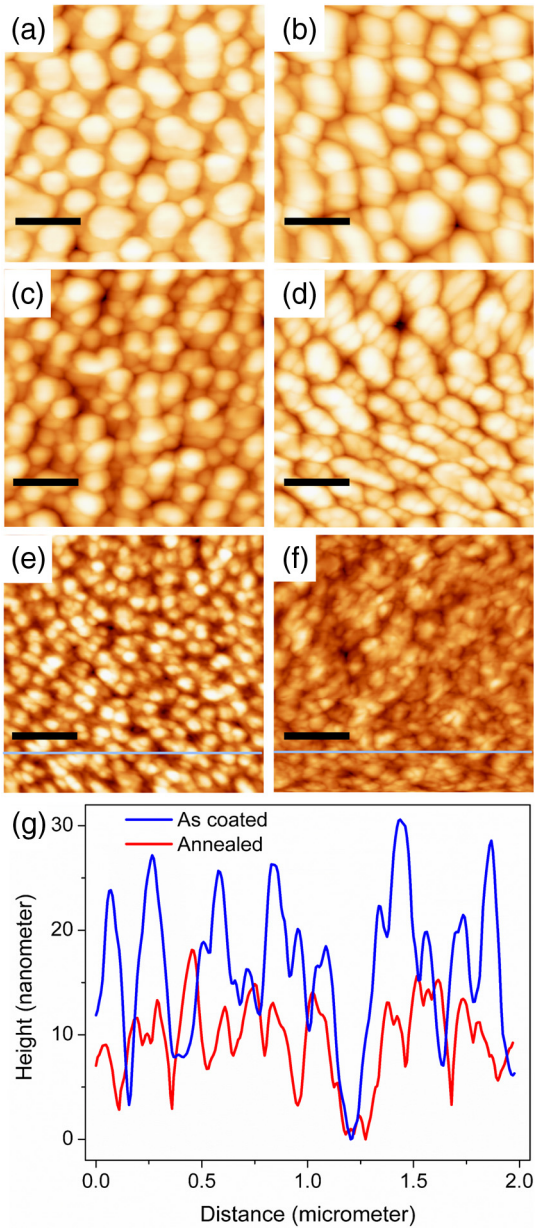

Fig. 9 AFM topography images of DPP-BZ:$PC_{71}BM$ blends: (a) and (b) with donor:acceptor (D:A) ratio of 1:2, z-scale of 95 nm, (c) and (d) with D:A ratio of 1:1.5, z-scale of 90 nm, (e) and (f) with D:A ratio of 1:0.7, z-scale of 40 nm. (a), (c), and (e) are as coated, and (b), (d), and (f) are annealed films. Scale bar = 0.5 μm. The height profile along the grey line of (e) and (f) is shown in (g).

D:A ratio) showed reduced performance mainly due to a decrease in J_{sc}. Upon annealing for 5 and 15 min, the J_{sc} was 4.0 mA/cm^2 and 3.9 mA/cm^2, respectively, which is ~10% lower than when annealed for 10 min. The PCEs for devices where the active layer was annealed for 5 and 10 min were 1.55 and 1.44%, respectively. Thermal annealing mainly affects the donor and acceptor crystallinity and their phase separation. Annealing at a particular temperature and for a specific time gives optimum phase separation and crystallinity and, hence, improved device performance. Devices annealed at higher temperatures also showed reduced J_{sc} and, hence, lower PCE. Figure 10 shows the absorption spectra of the blend films of various D:A ratios before and after thermal annealing at 110°C for 10 min. For the 1:0.7 ratio of DPP-BZ and $PC_{71}BM$, the J_{sc} and PCE obtained was 0.99 mA/cm^2 and 0.28% for the as coated photoactive layers. Upon thermal annealing at 110°C for 10 min, these improved to 4.42 mA/cm^2 and 1.76%, respectively. The shoulders/peaks corresponding to DPP-BZ absorption become prominent/sharp upon thermal annealing, which indicates improvement in the crystalline order in DPP. This, in turn, improves the charge carrier mobility in the donor phase. The absorption of the films in the visible region also increases. The AFM topography images indicate that the blend films become more compact and homogeneous upon thermal annealing. The above changes in the film properties upon thermal annealing result in large improvements in J_{sc} and FF and, hence, also in the PCE.[32,33] The inset in Fig. 8 shows the EQE of the best performing device. The quantum efficiency reaches a maximum of 28.2% at 615 nm. The DPP absorption in blend films is slightly blueshifted compared to that of pristine DPP films. The blueshift is more pronounced in films with a 1:2 D:A ratio compared to 1:0.7 D:A ratio blend films. It has been suggested that fullerene acceptors in the blend films distort the molecular packing of the donor polymer/small molecule and, thereby, decrease the effective conjugation length.[24,34] This effect would be larger for higher fullerene concentrations.

Another important parameter is the device thickness because it affects light absorption and charge extraction. The device performance parameters with different thicknesses of active layer for 1:0.7 D:A ratio are given in Table 3. Thermal annealing was performed at 110°C for 10 min. The best device efficiency was obtained for a 83-nm-thick active layer. For higher thicknesses, the J_{sc} and overall PCE decrease. The series resistance of the solar cell is contributed by three factors viz. the contact resistances between the different layers in the device, resistance of the top and rear metal contacts, and the resistance of the layers in the device including the BHJ active layer.[35] The series resistance increases with increasing active layer thickness. For an active layer thickness of 83 nm, the series resistance was 8 Ωcm^2, which increases to 18 Ωcm^2 for a 101 nm thickness and 40 Ωcm^2 for a 118-nm-thick active layer device. High series resistance reduces the current flow and also decreases the FF. Once the charges are separated at the D–A interface, the electric field created between the electrodes of different work functions sweeps these charges to the respective electrodes.[36] For larger thicknesses of the active layer, this field decreases, which, in turn, limits the charge transport toward the respective electrodes.

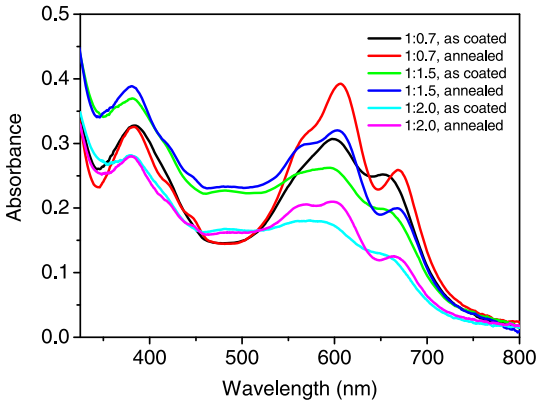

Fig. 10 Absorption spectra of DPP-BZ:$PC_{71}BM$ blends with and without thermal annealing.

Table 3 Device performance parameters of solar cells using DPP-BZ:$PC_{71}BM$ blends (1 : 0.7 D:A ratio) of different thicknesses.

Thickness (nm)	PCE (%)	J_{sc} (mA/cm^2)	V_{oc} (V)	FF (%)	R_s (Ωcm^2)
77	1.42	3.97	0.78	46.0	10
83	1.76	4.42	0.84	47.2	8
101	1.21	3.38	0.80	44.7	18
118	0.96	2.68	0.82	43.7	40

4 Conclusions

In conclusion, three DPP derivatives featuring electron-withdrawing units have been synthesized in respectable yields. Solution electrochemistry and DFT calculations have shown that these materials possess similar HOMO/LUMO energies and molecular orbital distributions. Solar cells have been fabricated with $PC_{71}BM$, which revealed that DPP-BZ gave the highest power conversion efficiency, while DPP-ES and DPP-AM devices had poor active layer morphology and hence low efficiency. The differences in device performance of the different materials can be explained by differences in the morphology seen in AFM measurements.

Acknowledgments

We are grateful to the EPSRC for funding (Grants EP/E036244 and EP/I00343X) and for use of the National Mass Spectrometry Facility, Swansea. I. D. W. S. is a Royal Society Wolfson Research Merit Award holder. S.S.G. thanks the North Maharashtra University, India, for providing study leave to do post-doctoral research at the University of St Andrews.

References

1. A. J. Heeger, "Bulk heterojunction solar cells: understanding the mechanism of operation," *Adv. Mater.* **26**(1), 10–28 (2014).
2. G. Li, R. Zhu, and Y. Yang, "Polymer solar cells," *Nat. Photonics* **6**, 153–161 (2012).
3. J. Roncali, P. Leriche, and P. Blanchard, "Molecular materials for organic photovoltaics: small is beautiful," *Adv. Mater.* **26**, 3821–3838 (2014);
4. A. F. Eftaiha et al., "Recent advances of non-fullerene, small molecular acceptors for solution processed bulk heterojunction solar cells," *J. Mater. Chem. A* **2**, 1201–1213 (2014);
5. Y. Chen, X. Wan, and G. Long, "High performance photovoltaic applications using solution-processed small molecules," *Acc. Chem. Res.* **46**(11), 2645–2655 (2013);
6. Y. Lin, Y. Lia, and X. Zhan, "Small molecule semiconductors for high-efficiency organic photovoltaics," *Chem. Soc. Rev.* **41**, 4245–4272 (2012);
7. A. Mishra and P. Bäuerle, "Small molecule organic semiconductors on the move: promises for future solar energy technology," *Angew. Chem. Int. Ed.* **51**(9), 2020–2067 (2012);
8. A. M. Raynor et al., "A diketopyrrolopyrrole and benzothiadiazole based small molecule electron acceptor: design, synthesis, characterization and photovoltaic properties," *RSC Adv.* **4**, 57635–57638 (2014).
9. D. Chandran and K. S. Lee, "Diketopyrrolopyrrole: a versatile building block for organic photovoltaic materials," *Macromol. Res.* **21**(3), 272–283 (2013);
10. Y. Li et al., "High mobility diketopyrrolopyrrole (DPP)-based organic semiconductor materials for organic thin film transistors and photovoltaics," *Energy Environ. Sci.* **6**, 1684–1710 (2013);
11. S. Qu and H. Tian, "Diketopyrrolopyrrole (DPP)-based materials for organic photovoltaics," *Chem. Commun.* **48**, 3039–3051 (2012);
12. M. A. Naik and S. Patil, "Diketopyrrolopyrrole-based conjugated polymers and small molecules for organic ambipolar transistors and solar cells," *J. Polym. Sci. A Polym. Chem.* **51**(20), 4241–4260 (2013).

13. S. Huang et al., "Preparation of sulfonamidophenylimidazolylpyrimidine derivatives and analogs for use as protein kinase inhibitors," WO 2011025927 A1 20110303 (2011).
14. A. Gupta et al., "Absorption enhancement of oligothiophene dyes through the use of a cyanopyridone acceptor group in solution-processed organic solar cells," *Chem. Commun.* **48**, 1889–1891 (2012).
15. C. H. Woo et al., "Incorporation of furan into low band-gap polymers for efficient solar cells," *J. Am. Chem. Soc.* **132**, 15547–15549 (2010).
16. J. Pommerehne et al., "Efficient two layer leds on a polymer blend basis," *Adv. Mater.* **7**, 551–554 (1995).
17. Spartan '08. Wavefunction, Inc.
18. A. Riaño et al., "The unusual electronic structure of ambipolar dicyanovinyl-substituted diketopyrrolopyrrole derivatives," *J. Mater. Chem. C* **2**(31), 6376–6386 (2014);
19. H. Wang et al., "The role of additive in diketopyrrolopyrrole-based small molecular bulk heterojunction solar cells," *Adv. Mater.* **25**(45), 6519–6525 (2013);
20. Y. Qiao et al., "Diketopyrrolopyrrole-containing quinoidal small molecules for high-performance, air-stable, and solution-processable n-channel organic field-effect transistors," *J. Am. Chem. Soc.* **134**(9), 4084–4087 (2012);
21. P. Sonar et al., "Solution processable low bandgap diketopyrrolopyrrole (DPP) based derivatives: novel acceptors for organic solar cells," *J. Mater. Chem.* **20**(18), 3626–3636 (2010);
22. B. P. Karsten, J. C. Bijleveld, and R. A. J. Janssen, "Diketopyrrolopyrroles as acceptor materials in organic photovoltaics," *Macromol. Rapid Commun.* **31**(17), 1554–1559 (2010).
23. Y. J. Kim et al., "Efficient diketopyrrolopyrrole-based small-molecule bulk-heterojunction solar cells with different electron-donating end-groups," *Chem. Asian J.* **9**(9), 2505–2513 (2014).
24. J. Huang et al., "Solution-processed DPP-based small molecule that gives high photovoltaic efficiency with judicious device optimization," *ACS Appl. Mater. Interfaces* **5**, 2033–2039 (2013).
25. O. Fenwick et al., "Efficient red electroluminescence from diketopyrrolopyrrole copolymerised with a polyfluorene," *APL Mater.* **1**, 032108 (2013).
26. Z. Masri et al., "Molecular weight dependence of exciton diffusion in poly(3-hexylthiophene)," *Adv. Energy Mater.* **3**(11), 1445–1453 (2013).
27. G. J. Hedley et al., "Determining the optimum morphology in high-performance polymer-fullerene organic photovoltaic cells," *Nat. Commun.* **4**, 2867 (2014).
28. J. Huang et al., "Fine-tuning device performances of small molecule solar cells via the more polarized DPP-attached donor units," *Phys. Chem. Chem. Phys.* **14**, 14238–14242 (2012).
29. C. J. Takacs et al., "Solar cell efficiency, self-assembly, and dipole–dipole interactions of isomorphic narrow-band-gap molecules," *J. Am. Chem. Soc.* **134**(40), 16597–16606 (2012).
30. Z. Xiao et al., "Hydrogen bonding in bulk heterojunction solar cells: a case study," *Sci. Rep.* **4**, 5701 (2014).
31. C. J. Novotny, E. T. Yu, and P. K. L. Yu, "InP nanowire/polymer hybrid photodiode," *Nano Lett.* **8**(3), 775–779 (2008).
32. O. P. Lee et al., "Efficient small molecule bulk heterojunction solar cells with high fill factors via pyrene-directed molecular self-assembly," *Adv. Mater.* **23**(45), 5359–5363 (2011).
33. C. M. Proctor et al., "Nongeminate recombination and charge transport limitations in diketopyrrolopyrrole-based solution-processed small molecule solar cells," *Adv. Funct. Mater.* **23**(28), 3584–3594 (2013).
34. J. Min et al., "Effects of oligothiophene π-bridge length on physical and photovoltaic properties of star-shaped molecules for bulk heterojunction solar cells," *J. Mater. Chem. A* **2**, 16135–16147 (2014).
35. R. A. Street, K. W. Song, and S. Cowan, "Influence of series resistance on the photocurrent analysis of organic solar cells," *Org. Electron.* **12**(2), 244–248 (2011).
36. T. Ameri, N. Li, and C. J. Brabec, "Highly efficient organic tandem solar cells: a follow up review," *Energy Environ. Sci.* **6**, 2390–2413 (2013).

Sanjay S. Ghosh received his PhD in physics/materials science from the University of Pune, India, in 2013. Thereafter, in January 2014, he joined the group of Professor Ifor Samuel as a

postdoctoral research fellow. Currently, he is working as an assistant professor in the Department of Physics, North Maharashtra University, India.

Luis A. Serrano received his BSc honors degree in chemistry from the University of Extremadura and the University of the West of Scotland in 2011. He is currently completing his PhD on the subject of synthesis of redox-active materials with photoelectronic properties in the group of Professor Graeme Cooke.

Bernd Ebenhoch is currently completing his PhD on the subject of organic solar cells—novel materials, charge transport, and plasmonic studies, in the group of Professor Ifor Samuel.

Vincent M. Rotello is the Goessmann professor of chemistry and university distinguished professor at the University of Massachusetts–Amherst. He joined UMass in 1993, and received the NSF CAREER, Cottrell Scholar, and Camille Dreyfus Teacher-Scholar awards, the Sloan Fellowship, and the Langmuir Lectureship, and is a fellow of the AAAS and the Royal Society of Chemistry (United Kingdom). His research program focuses on engineering the interface between hard and soft materials, with >430 papers published to date.

Graeme Cooke is a professor of physical organic chemistry and head of nanoscience and materials chemistry within the School of Chemistry at the University of Glasgow. He is currently director of the Scottish Institute for Solar Energy Research (SISER). His research focuses on the design, synthesis, characterization, and self-assembly of functional molecules, polymers, and nanoparticles. He has published >120 papers to date.

Ifor D. W. Samuel is professor of Physics and Director of the Organic Semiconductor Centre at the University of St Andrews. He received his MA and PhD from the University of Cambridge, performed postdoctoral research at CNET-France Telecom in Paris, and set up the light-emitting polymer research group at the University of Durham before moving to St Andrews. He is a fellow of the Royal Society of Edinburgh, the Institute of Physics, the Royal Society of Chemistry and SPIE.